Bone-Inspired Materials by Design: Toughness Amplification Observed Using 3D Printing and Testing**

By *Flavia Libonati, Grace X. Gu, Zhao Qin, Laura Vergani* and *Markus J. Buehler**

Inspired by the fact that nature provides multifunctional composites by using universal building blocks, the authors design and test synthetic composites with a pattern inspired by the microstructure of cortical bone. Using a high-resolution multimaterial 3D printer, the authors are able to manufacture samples and investigate their fracture behavior in mechanical tests. The authors' results demonstrate that the bone-inspired design is critical for toughness amplification and balance with material strength. The failure modes of the authors' synthetic composites show similarities with the cortical bone, like crack deflection and branching, constrained microcracking, and fibril bridging. The authors' results confirm that our design is eligible to reproduce the fracture and toughening mechanism of bone.

1. Introduction

The last decades have seen an increasing use of composites for load-bearing structural applications because these materials can lead to lightweight structures with great mechanical properties in terms of strength and stiffness. The combination of such properties with a low density is sought-after in a variety of strategic fields, such as biomedicine, buildings, transportations, and energy storage. However, the relatively low toughness of some composite materials is often of great concern, as it can cause sudden rupture. Tough materials, instead, absorb a lot of energy as a crack grows through them, preventing the case of catastrophic sudden failure. Lately, scientists and engineers tried to overcome this limitation by mimicking nature, yielding to a new class of composites with improved mechanical properties: the biomimetic composites.[1–12]

Biomimicry has led to many innovations that strongly influence how we design materials and products, such as gecko-inspired dry structural adhesives,[13,14] lotus leaf-inspired self-cleaning materials,[15,16] and nacre-inspired damage-tolerant nanocomposites.[3–6] Natural composites are a good source of inspiration for the design of new smart materials and continuously attract many researchers. A peculiarity of such materials is their hierarchical structure, which generally spawns lightweight composites with mechanical properties far superior to those of their constituents.[17–21] A classic example is bone, made of apparently meager constituents but resulting in a lightweight structural material with unique strength and toughness combination.

Researchers put a lot of effort into understanding the hierarchical structure of natural materials and its effects on the mechanical properties, at different length scales. To date, different approaches, both numerical and experimental, have been adopted to understand properties at multiple length scales. Among numerical methods, atomistic-to-continuum simulations have been used to elucidate the nature principles behind the superior mechanical performance of such materials,[22–25] leading to discover the key role played by the nanometer scale to achieve flaw tolerance and superior properties in most biological systems.[23]

Mimicking the features of natural materials is non-trivial and few scientists successfully reproduced the key mechanisms underlying the mechanical characteristics. For instance, freeze casting has proven to be an effective and versatile manufacturing

[*] *Dr. M. J. Buehler, Dr. F. Libonati, G. X. Gu, Dr. Z. Qin*
Laboratory for Atomistic and Molecular Mechanics (LAMM), Department of Civil and Environmental Engineering, Massachusetts Institute of Technology, 77 Massachusetts Ave., Cambridge, Massachusetts 02139, USA
E-mail: mbuehler@mit.edu
Dr. F. Libonati, Dr. L. Vergani
Politecnico di Milano, via La Masa 1, 20156 Milano, Italy

[**] *We acknowledge support from "Progetto Rocca – MISTI Global seed funds." We would like to thank the technicians Luca Signorelli and Lorenzo Giudici (from Politecnico di Milano) for their help with the experimental testing. GXG, ZQ, and MJB acknowledge support from Naval Research (N000141010562) and DURIP (PA-AFOSR-2013-0001). GXG acknowledges support from National Defense Science and Engineering Graduate fellowship (NDSEG) Program. Additional support from BASF-NORA is also acknowledged.*

process to create damage-tolerant nacre-like composites.[4,5,26–28] An excellent example of effective biomimetic design is given by Chen et al.,[6] who fabricated a composite paper, made of graphene oxide (GO)/sodium alginate (SA) building blocks, by mimicking the hybrid structure of natural nacre. By enhancing the H-bond formation between the two base materials, they reached a perfect combination of high strength and toughness, surpassing the properties of natural nacre and other similar composites. Classical lamination techniques have also been used to create innovative bio-inspired composites at a larger scale. Indeed, in a recent study, Libonati et al.,[29] successfully replicated some of the microscale toughening mechanisms occurring in cortical bone in a de novo FRC (fiber-reinforced composite).

In the last years, the rapid growth of additive manufacturing has led to many innovative biomimetic composites: i) Dimas et al.[30] developed new composites inspired by bio-mineralized materials with tunable fracture mechanics properties and used computational models to predict the fracture response; ii) Lin et al.[31] used analytical models and experiments on 3D-printed polymer prototypes to investigate the deformation and failure mechanisms of different suture interface geometries; iii) Zhang et al.[32] developed bio-inspired staggered composites with enhanced energy dissipation through a numerical-experimental approach; iv) Qin et al.[33] combined 3D printing with computational modeling to design and synthesize man-made spider webs with optimized strength. Recent advances in additive manufacturing have also enabled 3D printing of biocompatible materials, cells, scaffolds, and living tissues. This technique, known as 3D bio-printing, is driving a major challenge in both engineering and medical fields.[34,35]

In this work, we use additive manufacturing as a rapid and effective technique to create bone-like polymer composites with improved fracture toughness and strength–toughness balance with respect to the base constituents. In particular, as nature uses few universal building blocks to achieve unique functional properties through hierarchies, with a similar approach we use pure polymers as building blocks to investigate, through bio-inspired design, the effect of different geometries (Figure 1) and to get property improvement. We believe that the amplification in toughness occurring in bone is mainly due to the structural organization and fracture mechanisms characteristic of each hierarchical level. Our goal is to achieve such increase in toughness mimicking the fundamental microscale toughening mechanisms, by reproducing the key microstructural features actively involved in the fracture process – the osteons. In the following, we demonstrate how to obtain an effective combination of strength and toughness in composites, despite the material limitations of 3D printing, through a biomimetic approach.

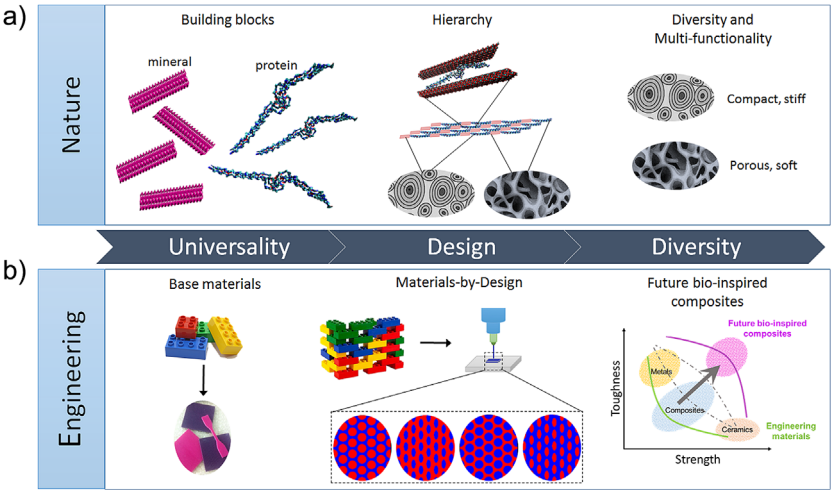

Fig. 1. Comparison between nature and engineering approach. (a) In nature exists universal building blocks, such as minerals and proteins, which combine to form different materials, e.g., bone. In bone, we can distinguish different structures through hierarchy. Each structure evolves and adapts to meet specific functions in the body (e.g., cortical bone has a compact structure, providing structural support, whereas trabecular one has a porous structure, providing compression resistance and promoting the remodeling process through the cells contained in the pores). (b) Engineers can use a wide variety of materials, belonging to different classes (i.e., metals, ceramic, and plastics). Here, we use pure polymers as base materials and we probe, through 3D printing, the effect of different bone-inspired geometries. We chose bone as biomimetic model for its large amplification in toughness with respect to its building blocks and for its remarkable strength–toughness balance. With a similar approach, we aim to design future bio-inspired composites with an optimal strength–toughness balance and a toughness enhancement with respect to the basic constituents.

2. Inspiration and Design

For the design, we followed a biomimetic approach, borrowing inspiration from bone. Indeed, among natural materials, bone is a promising candidate: its hierarchical lightweight structure provides support to a wide class of animal bodies. The great combination of mechanical properties, in particular the strength-to-weight and stiffness-to-weight ratios, and the outstanding toughness, makes it very attractive for research studies. In particular, bone has a remarkable fracture toughness, which far exceeds that of its basic building blocks (about three to five order of magnitude).[17] The origin of bone toughness lies in the multiple toughening mechanisms activated at different length scales, from nanoscale collagen fibril bridging to microscale crack deflection.[36] It has been revealed that all the hierarchical structural features synergistically contribute to the mechanics of bone and help to dissipate the energy during fracture. However, totally replicating the bone structure and mechanics may need to involve several techniques at different length scales including genetic engineering, molecular self-assembly, material deposition, and so forth. Here, we do not aim to study the entire hierarchical structure of bone from atomic level and up, but we focus on the Haversian structure (characteristic of microstructural level of cortical bone), where the crucial mechanisms, such as crack deflection, occur. The latter, enhanced by the presence of large microstructural cylindrical features, called osteons, is thought to cause a major

increase in the overall bone fracture toughness.[37] Osteons are made of circumferential lamellae to form a circular-to-elliptical cross-section, and have an apparently random distribution, resulting from the stress-induced remodeling process. They are surrounded by the interstitial matrix, made of interstitial lamellae. Owing to their geometry and to different properties than the matrix (i.e., the osteon–matrix stiffness ratio is about 0.64),[38] they create stress delocalization, reducing the local stresses at the crack tip and resulting in crack shielding. Also, the osteon outer boundaries, called cement lines, are dense of microcracks, allowing for additional energy dissipation.[39] The Haversian structure is characteristic of many animals and the osteon density and distribution is correlated to the stress distribution.[40] Indeed, animals subjected to stresses that come from gravity force, such as human, bovine, and equine species show a characteristic osteonal structure, whereas fish species are characterized by a more lamellar one.[41] It has been shown that energy dissipation arising from the bone heterogeneity lead to markedly different biomechanical properties compared with a uniform material.[42] This is a common characteristic of a broad class of biological materials and may serve as a design guideline for biologically inspired composites, using multi-material technology.

In this study, we are mainly interested in implementing the mechanisms of how bone amplifies toughness with respect to its basic building blocks to de novo composite designs by simply replicating some microstructural features, the osteons. We designed simplified models of a bone-like structure, mimicking the osteons, which represent the reinforcement, as cylinders embedded into a matrix. In the 3D-printed composite materials, we did not fabricate the outer boundaries aimed at mimicking the cement lines. Indeed, our initial designs are simplified versions of the Haversian structure because we decided to start with a simple representation of the bone microstructure and study the effect of two parameters (geometry and materials). In Figure 2a, we show the material design process, the manufacturing process, the final samples, and the testing setup. We investigated: i) the role of the reinforcement (i.e., osteon) geometry, simplifying the osteons as circular and elliptical, ii) the role of the osteon direction, by performing tests in two orthogonal directions, and iii) the role of the reinforcement/matrix stiffness ratio, by considering the case of stiff reinforcement and soft matrix and the opposite one. The case of stiff matrix and soft reinforcement is more similar to the case of bone, where the interstitial matrix is generally more mineralized, hence, stiffer than the osteons. In all the case studies, we paid attention to keep a constant osteon volume ratio, defined as the ratio between the volume of the osteons and that of the interstitial matrix, and equal to 60%. We chose this value as an average from the

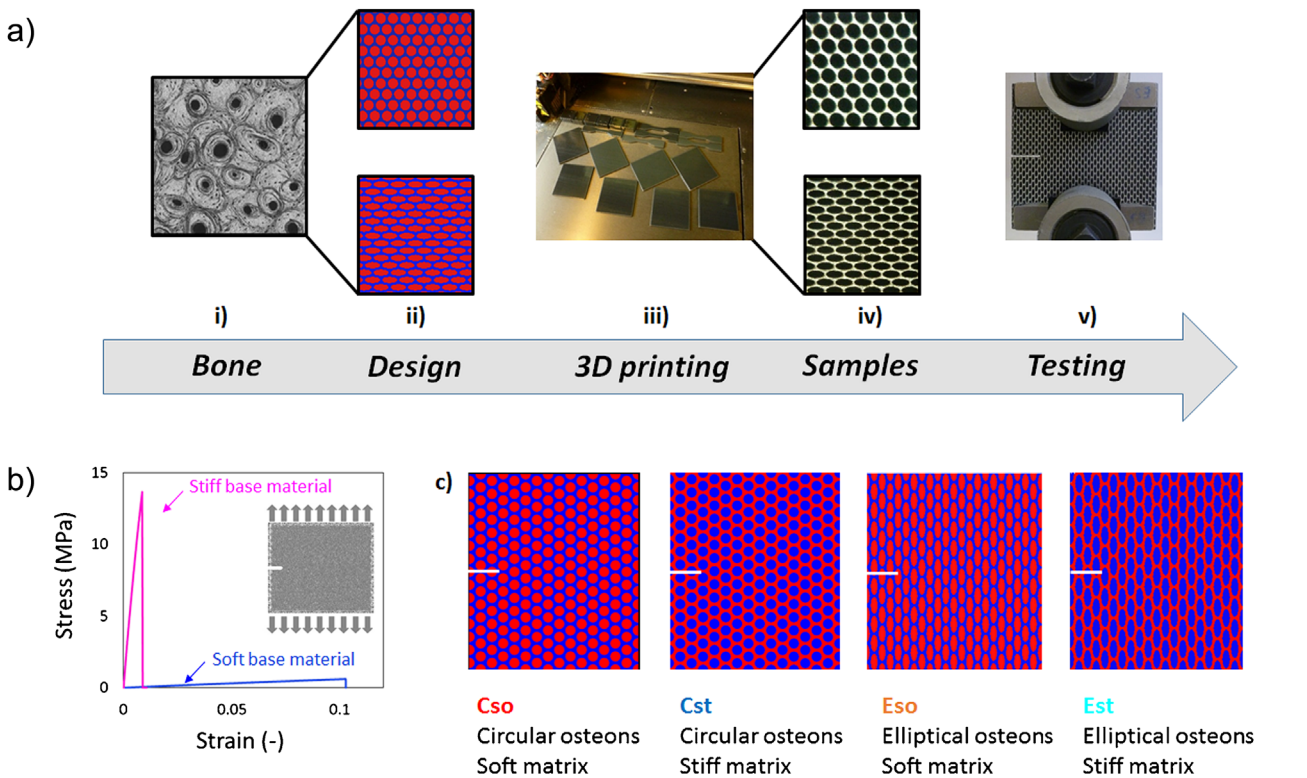

Fig. 2. (a) Biomimetic approach: i) inspiration from the microstructure of cortical bone (i.e., Haversian structure), ii) design of different material topologies, iii) 3D printing, iv) printed samples, v) testing setup. We design simplified version of composite materials inspired by the microstructure of cortical bone, by keeping the osteon volume ratio equal to 60%, as in cortical bone. We mimic the fundamental microstructural features, the osteon, as circular-to-elliptical inclusions. We investigate the effect of the reinforcement/matrix stiffness ratio, by manufacturing and testing samples with both stiff reinforcement/soft matrix and soft reinforcement/stiff matrix. (b) Schematic of the sample geometry, applied loading condition, and corresponding stress–strain curves for the base materials. There is a clear difference between the two base materials: the stiff materials are characterized by a high stiffness and strength, whereas the compliant ones are characterized by a high ability to strain. (c) Types of composites: Cso, made of circular osteons and soft matrix; Cst, made of circular osteons and stiff matrix; Eso, made of elliptical osteons and soft matrix; Est, made of elliptical osteons and stiff matrix.

literature – experimentally found to be about 60% in bovine bone.[38,43] We should point out that in our materials we did not replicate the same osteon/matrix stiffness ratio found in cortical bone, but we chose highly contrasting material properties to clearly see the effect of the geometry and stiffness ratio. We chose the size of the osteons to include, in future works, the cement line. We tried to keep the same size of the features of real bone: in real bone, the osteon diameter is included in the range 100–300 μm and the cement line is included in the range 4–7 μm. Considering the resolution of the printer (i.e., 16 μm) and in view of printing, in future composites, the cement line too, we decided to adopt the same dimension for the osteon diameter, but increasing it by one order of magnitude. This will allow us to print future composites including the cement lines, and maintaining the same osteon diameter, also allowing a direct comparison with the present data. Regarding the geometry of the inclusions, we simplified the osteon as circular and elliptical. Indeed, in the literature, osteons have a circular-elliptical cross-section, and generally the ellipse has an aspect ratio (i.e., minor axis/major axis) included in the range 0.4–0.8. Here, we chose an aspect ratio of 0.5 to investigate the effect of geometrical difference (between the elliptical and the circular case) and that of the anisotropy. In the future, the effect of different aspect ratios could be object of further studies.

3. Results

We first characterized the base polymer materials, and then we proceeded to study the deformation and fracture mechanisms of the bone-inspired composites. All the composites are made of the same base materials, representing the building blocks, and have the same geometry and loading condition, to allow a final comparison. The schematic of the sample geometry and loading conditions used for fracture testing is shown in Figure 2b, along with the experimental stress–strain curves of the base materials. In Figure 2c, we show all the topologies of composites used for fracture testing. More details are provided in the Experimental Section.

3.1. Failure Modes and Comparison with Bone Tissue

In all the composites, we notice a clear effect of the microstructure on the crack propagation and on the overall failure mode. In all the cases, as the load is applied, stress concentration at notch tip is reduced by the stress delocalization from the reinforcement pattern. The crack path is nonlinear and strongly affected by the geometry. Moreover, as highlighted in the Experimental Section, no failure occurs at the reinforcement/matrix interface, confirming a perfect adhesion between the two base materials, which is due to in situ curing, characteristic of the adopted multimaterial 3D printing technology.

In the case of samples with elliptical reinforcement and soft matrix, we observe a characteristic zigzag crack path, due to continuous crack branching, as shown in Figure 3a. For this type of composite, the main toughening mechanism is crack branching. We can observe the crack-blunting phenomenon, followed by a characteristic crack scissoring. The crack splits into two branches and the main one propagates until a second splitting occurs. This mechanism continuously repeats until the final failure.

In the case of samples with circular reinforcement and soft matrix, the crack follows the osteon boundaries showing a characteristic toothed crack path, due to continuous osteon-driven crack deviations, as shown in Figure 3b. In this case, the main toughening mechanism is crack deflection. In both cases represented in Figure 3a and b, significant deformations and additional dissipation mechanisms occur into the compliant phase, further increasing the energy dissipation before fracture. In particular, formation of microvoids into the matrix, ahead the crack tip, reducing the stress concentration at the crack tip, and fibril bridging behind the crack tip. Both mechanisms reduce the crack growth rate, preventing a quick failure. The difference in the crack path and main propagation mechanism (between the case reported in Figure 3a and b) is due to the different osteon geometry (elliptical and circular, respectively).

By observing the failure mechanisms of the composites made of stiff matrix and soft reinforcement, we notice a minor effect of the reinforcement geometry on the crack propagation.

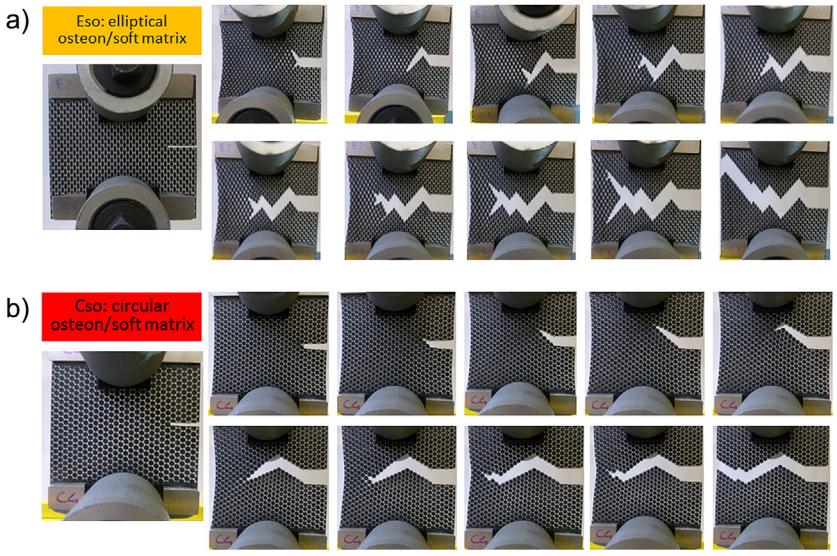

Fig. 3. (a) Snapshots of the failure modes of samples with elliptical reinforcement and soft matrix. We observe a characteristic zigzag crack path, owing to continuous crack branching. For this type of composite, the main toughening mechanism is crack branching. (b) Snapshots of the failure modes of samples with circular reinforcement and soft matrix. We observe a characteristic jagged crack path, owing to continuous osteon-driven crack deflections. In this case, the main toughening mechanism is crack deflection. In both cases, shown in subplots (a) and (b), significant deformations occur in the compliant phase: in particular, formation of microvoids into the matrix, ahead the crack tip, reducing the stress concentration and fibril bridging behind the crack tip, preventing crack propagation. Both mechanisms reduce the crack growth rate, preventing a quick failure.

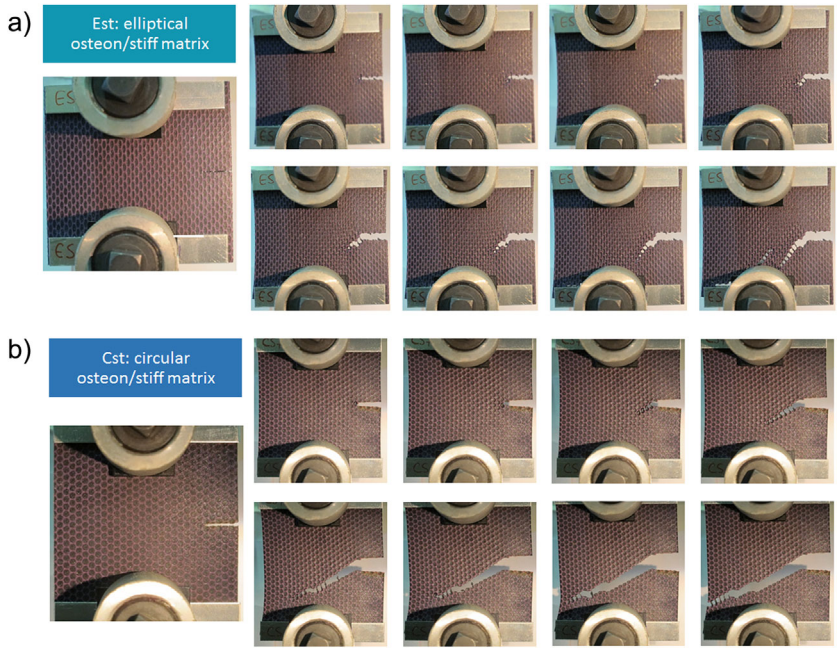

Fig. 4. (a) Snapshots of the failure modes of samples with elliptical reinforcement and stiff matrix. (b) Snapshots of the failure modes of samples with circular reinforcement and stiff matrix. In both cases, shown in subplots (a) and (b), we observe an irregular crack path, influenced by the composite pattern. Large deformations occur in the soft inclusions. The deformation of the osteon-like inclusion and the formation of many tiny cracks into the stiff matrix reduce the stresses at the crack tip. The tiny cracks are not connected, and the load is carried through uncracked-ligament bridging. Fibril bridging occurs behind the crack tip, inhibiting a fast crack growth.

In both cases, reported in Figure 4a and b we observe large deformation into the soft inclusions and the formation of many tiny cracks into the stiff matrix, which both reduce the stresses at the crack tip. The tiny cracks are not connected, and the load is carried through uncracked-ligament bridging. In addition, fibril bridging occurs behind the crack tip, inhibiting a fast crack growth and preventing a catastrophic failure.

The effect of stiffness ratio strongly affects the crack propagation and the overall failure mode. In particular, in the case of stiff inclusions and soft matrix, the effect of the osteon geometry is more evident. Here, the matrix is more compliant, the inclusions carry out most of the load, and the crack path follows the inclusion boundaries. We can distinguish the key toughening mechanisms: crack branching, for the elliptical pattern (Figure 3a), and crack deviation, for the circular one (Figure 3b). When the matrix is stiffer than the inclusions, instead, the effect of the inclusion geometry is not clear in terms of failure mode, but in terms of mechanical properties. The matrix carries most of the load. In addition, the matrix surrounds the inclusions and being less deformable, it acts as constraint, preventing the initial deformation of the inclusions that behave in the same way, irrespective of the geometry. Here, the most important toughening mechanisms of all the samples characterized by a stiff matrix are uncracked ligament bridging, occurring in the stiff matrix, and fibril bridging, occurring in the soft inclusions. On the contrary, the effect of the inclusion geometry is clear on the overall mechanical properties and the elliptical one is shown to be the most successful case (see Section 3.2).

In our 3D-printed composites, we recognize several toughening mechanisms similar to those occurring in bone microstructure, as shown in Figure 5, where a comparison between the principal toughening mechanisms occurring in

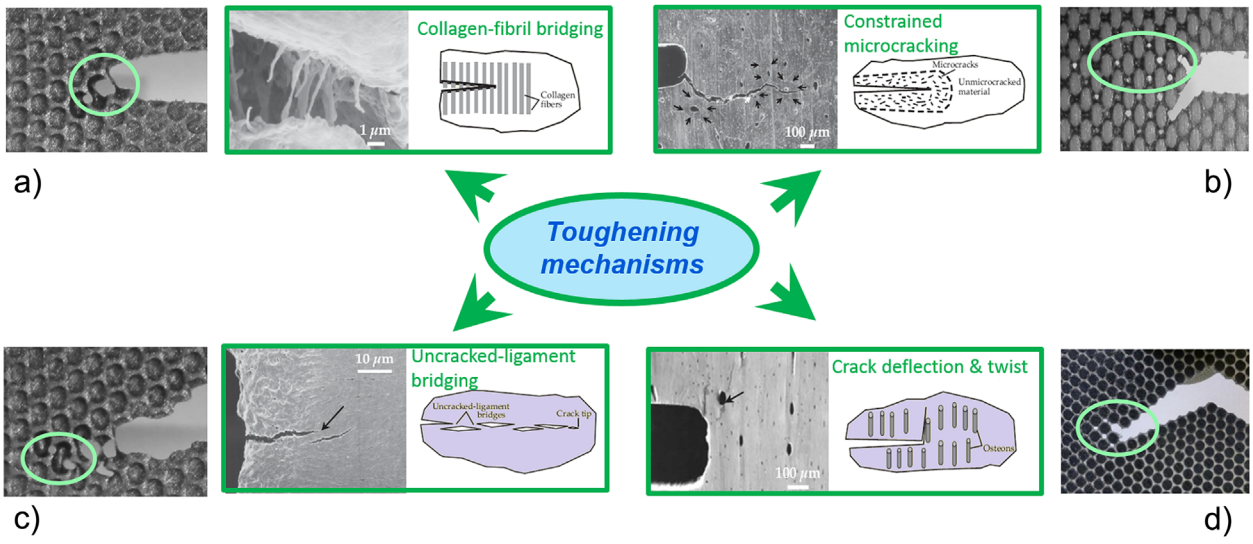

Fig. 5. Principal toughening mechanisms occurring in our bone-inspired composites and comparison with those occurring in the microstructure of cortical bone. Adapted with permission from ref.,[37] copyright (2009), American Institute of Physics. In our 3D-printed composites, we recognize several toughening mechanisms similar to those occurring in bone. Small-scale mechanisms: (a) fibril bridging, occurring in the soft phase, (b) formation of microvoids and microcracks, occurring ahead the crack tip, and (c) uncracked-ligament bridging. Large-scale mechanisms: (d) crack deviation.

our bone-inspired composites and those occurring in the microstructure of cortical bone[37] is given. In particular:

i) *Small-scale mechanisms*, such as formation of microvoids and microcracks, occurring ahead the crack tip, in the soft and stiff phase, respectively; also, fibril bridging, always occurring in the soft phase, and uncracked ligament bridging.
ii) *Large-scale mechanisms*, such as crack blunting, crack branching, and crack deviation around the osteons.

All these mechanisms contribute to dissipate the energy during the failure process, considerably increasing the composite toughness compared to their building blocks.

3.2. Amplification in Toughness and Optimal Strength–Toughness Balance Achieved by the Bone-Inspired Composite

The use of the same sample geometry and loading conditions in the fracture toughness tests allow us to compare the stiffness, strength, toughness, and strain between the base materials and the new composites. We notice a wide range of stress–strain behaviors, though the materials are made of the same building blocks and the same reinforcement ratio. Specifically, by comparing the mechanical properties, we observe an increase in toughness of the composites compared to the base materials, almost one order of magnitude. This is clear from the radar plots, in Figure 6a and b, showing a comparison among all the topologies of samples. Data are normalized by the maximum value of each mechanical characteristic. In Figure 6a, the radar plot shows a comparison between the base materials and all the composite topologies. In Figure 6b, instead, the radar plot shows a comparison among all the composite topologies. It is evident from these graphs, that the "Est" composite type (i.e., soft elliptical reinforcement/stiff matrix) has the best combination of mechanical properties (i.e., strength, toughness, stiffness, and strain), which is measured as the proportional area of the radar plots.

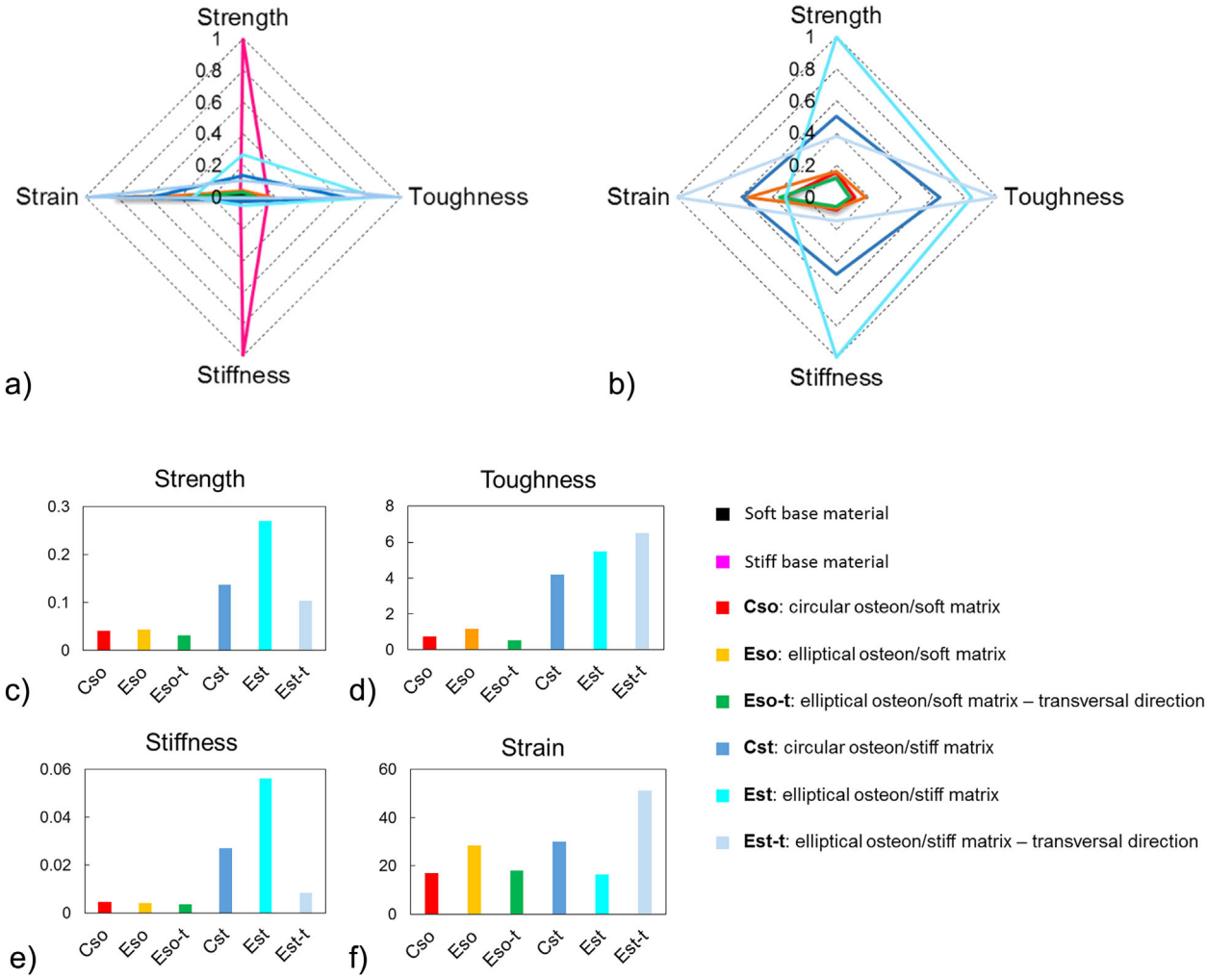

Fig. 6. (a, b) Radar plots showing a comparison among all the topologies of samples. Data are normalized by the maximum value of each mechanical characteristic. (a) Radar plot showing the base materials and all the composites. (b) Radar plot showing a comparison among all the composite topologies. The "Est" composite type (i.e., soft reinforcement/stiff matrix and elliptical osteon geometry) has the best combination of mechanical properties (i.e., strength, toughness, stiffness, and strain), measured as the proportional area of the radar plots. (c, f) Bar plots: comparison among all the topologies of samples. Data are normalized by the respective value of the stiff base material for each mechanical characteristic: (c) strength, (d) toughness, (e) stiffness, and (f) strain. The best performance is given by "Est" composites (i.e., soft reinforcement/stiff matrix and elliptical osteon geometry), either in longitudinal and transversal directions. This type of composite shows the best combination of strength and toughness, ensuring a high stiffness and a good deformability.

The bar plots, represented in Figure 6c–f, allow us to make a comparison among all the topologies of composites, on each mechanical property. Here, the data are normalized by the respective value of the stiff base material for each mechanical characteristic, allowing a direct comparison between each composite and the stiffer–stronger building block. The "Est" composite topology shows the best performance in terms of strength and stiffness, in longitudinal direction, and in terms of toughness and strain in transversal direction. Moreover, this material shows a consistent amplification in toughness, about 15 and 7 times higher than the soft and stiff materials, respectively. The amplification in toughness with respect to the basic constituents is a remarkable property of bone, as shown in the Ashby plot (Figure 7a). With a bone-inspired design, we were able to mimic this characteristic (Figure 7b), by mimicking the fundamental toughening mechanisms.

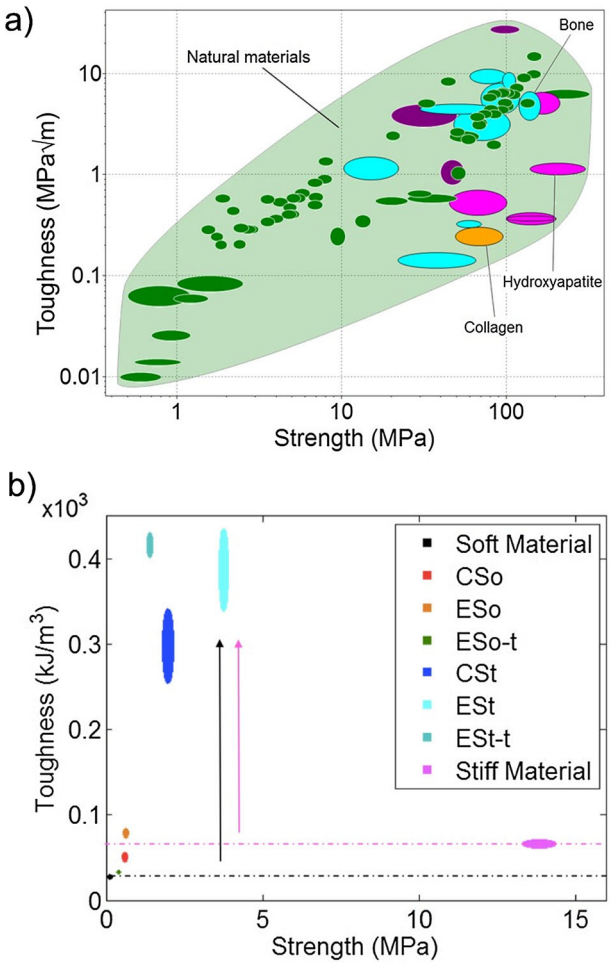

Fig. 7. (a) Ashby plot showing the mechanical properties of natural materials. Highlighted bone and its basic building blocks, collagen and hydroxyapatite. The plot shows the large amplification in toughness of bone with respect to its basic constituents. (b) Ashby plot summarizing the experimental results from the 3D-printed bone-inspired composites. The composites characterized by a stiff matrix show an amplification in toughness with respect to the basic constituents. The "Est" composite type (i.e., soft reinforcement/stiff matrix and elliptical osteon geometry) shows the best amplification in toughness, in both longitudinal and transversal directions. The colored arrows show the increase in toughness of the composites with respect to the base materials (whose toughness level is highlighted by the colored-dashed lines).

This result is comparable to that achieved by Dimas et al.,[30] who synthetized brick-and-mortar biocalcite- and bone-like structures, after developing mesoscale models.[19,44] Dimas et al.[30] also achieved an increase in toughness about one order of magnitude and mechanical performance far superior to their constituents, by mimicking different toughening mechanisms, common to various biominerals at nanoscale. Here, we use similar polymer base materials, but we mimic a different pattern, showing different toughening mechanisms. Moreover, the previous paper by Dimas et al. focuses on the mechanism of the enhanced toughness of multi-material composites, while the current work focuses on the design of composite materials of multiple mechanical functions. This work is focusing on a different structure (i.e., the microstructure) and the authors are trying to create de novo bone-like composites by using different techniques. Indeed, an alternative approach is shown in ref.,[29] where Libonati et al. used composite lamination to develop a biomimetic composite inspired by the microstructure of cortical bone. Another difference, which makes the present results not directly comparable with those presented in ref.,[30] is the volume fraction of the stiff phase, 60% in the present study, compared to 80% in ref.[30] In both studies, the bone-like topology has shown to be a successful choice, leading to damage-tolerant composites with mechanical performance far superior to their building blocks. In the composites, the characteristic bio-inspired pattern reduces the stress concentration around the crack tip, driving the strain transfer in the compliant phase and the stress transfer in the stiff one. This makes the composites less sensitive to the presence of flaws, thus leading to a non-catastrophic failure mode, characterized by a stable crack propagation.

4. Conclusion

In this work, we showed the importance of the geometrical features of cortical bone in determining the fracture toughness, by activating some of the toughening mechanisms, characteristic of the microstructure. Our results show how to successfully achieve an amplification in toughness and mimic the fundamental toughening mechanisms of cortical bone, by replicating the major microstructural features. The rationale of this work was to examine the biomimetic design principles to develop damage-tolerant lightweight composites, with enhanced properties than their building blocks, and use 3D printing as proof of concept. With respect to previous literature studies,[3,5,6,19,30,44] which aimed to replicate the biominerals and their characteristic fracture mechanisms, here we used an empirical biomimetic approach and we focused on bone and on its characteristic Haversian structure, which plays a major role in activating the fundamental toughening mechanisms.

The results from this study reveal an important role, played by the osteon-like reinforcements. In particular, such inclusions: i) modify the stress state in the matrix reducing

the stress concentration at the crack tip and making the composites less sensitive to the presence of flaws; ii) cause the formation of stress-induced microvoids/microcracks (acting as dissipative mechanism) in the matrix; iii) promote a stable crack propagation, characterized by a non-linear crack path, due to crack deviation for the circular reinforcement/soft matrix case, and to crack branching for the elliptical reinforcement/soft matrix one; and iv) increase the toughness of the composites up to one order of magnitude with respect to their building blocks. This study shows that among all the new designs, the one with elliptical soft inclusions and stiff matrix gives the best improvement of mechanical properties, compared to the base materials, as it occurs in bone tissue, where the matrix is stiffer, due to a higher degree of mineralization. Additionally, mentioned in the literature, osteons are generally schematized as circular. However, in reality their cross-sectional geometry is elliptical, and the eccentricity is related to its age. Indeed, it has been found that the eccentricity decreases with age, meaning that the osteons tend to become less elliptical.[45] Elliptical osteons are then characteristic of a young and stronger bone. Hence, we expected a better behavior (in terms of strength and toughness) of the composites with elliptical inclusions compared to the circular ones, as confirmed by these results. Our findings also demonstrate that the in situ UV curing ensures a perfect adhesion between the reinforcement and the matrix, since no interfacial debonding occurred in the composites. Also, we should note that in our composites it is very likely that the inclusion/matrix interface has different properties than those of the base materials. Indeed, during the UV-curing process it is possible that a mixture of the two materials occurred at the interface, leading to a third component, which could have the role of cement lines.

In future work, we will consider new designs, based on random geometry, orientation, and size of the osteons. We will also take advantage of the dual jetting material technology, to print new samples with the matrix and the inclusions made of the same building blocks as in bone, by using a mixture of the two base materials, and to print a third component to mimic the cement lines. Being the cement lines dense of microcracks, which allow for additional energy dissipation, we aim to implement this feature in future composites by introducing local defects in the inclusion outer boundaries. Moreover, this technology will be used to balance the stiffness ratio (using a mixture of the two base materials) to reach less contrasting properties between the matrix and the inclusions, as in bone. Computational modeling will be helpful in finding the optimal ratio between the base materials and the optimal geometrical configuration.

Additive manufacturing has shown to be a disruptive technique that can potentially revolutionize many industries. Successful examples arise from laboratory research, as we show in this paper. However, the main challenge is to scale-up these innovative materials in practical applications.

5. Experimental Section

5.1. Design and Manufacturing

We designed the pattern of all the samples using AutoCAD (Autodesk, Inc.). For composite printing, we used the following base materials: VeroBlackPlus (RGD875) and VeroMagenta (RGD851) as stiff materials, and TangoPlus (FLX930) and TangoBlackPlus (FLX980) as compliant materials. Both the Vero-materials and the Tango-materials are acrylic-based photopolymers. We chose materials with high contrasting properties, whose stiffness differs by three orders of magnitude, and the strain at breakage by one order of magnitude.

We manufactured the VeroBlackPlus/TangoPlus composites in the Precision Compliant System Lab (PCSL) at MIT using an Objet500 Connex 2 multi-material 3D printer by Stratasys, and the VeroMagenta/TangoBlackPlus composites in the LAMM at MIT, using an Objet500 Connex 3 multi-material 3D printer. Both printers employ multimaterial 3D printing technology, in which printing heads jet out materials that are immediately cured with UV light. Moreover, the printers allow printing two different materials simultaneously. The materials adopted and the process (PolyJet) are exactly the same for both printers, as reported on the website of the producer, so we firmly think that no further variables have been added to the experimental setup. Since the materials cure in situ, during manufacturing, a perfect reinforcement/matrix adhesion is guaranteed in the composites. This was confirmed during testing, since no interface failure occurred. Miscibility is also ensured by the manufacturer. According to the manufacturer, all the materials are miscible and different combinations of them can also be printed. Indeed, for some combinations, known as Digital Materials,[46] the manufacturer also provides the data sheet with the mechanical properties. In the pre-processing step, we used a software that automatically calculates the placement of photopolymers and support material from a 3D CAD file. After printing, we used a water jet to remove the gel-like support material from the samples.

5.2. Characterization of the Base Material under Static Loading

To characterize the stiff base materials under tensile loading, we printed dogbone samples, with geometry and size according to the standard ASTM D638,[47] which defines the test method for tensile properties of plastics. For the compliant base material we followed the standard ASTM D412,[48] which defines the test methods for tensile properties of vulcanized rubber and thermoplastic elastomers. For the testing setup, we followed the above-mentioned standards.[47,48]

We performed tensile tests on at least three stiff material samples using an MTS Alliance RT-100 universal tensile testing machine, endowed with a 100 kN load cell, and a 5 mm min^{-1} crosshead speed. For the stiffer samples, we also adopted an MTS 634.25F-54 extensometer with a 50 mm gauge length. For tensile testing of soft materials, we used an MTS Synergie 200 universal tensile testing machine, endowed with a 1 kN load cell. We carried out tests in displacement control, using a 500 mm min^{-1} crosshead speed. For all the tensile tests, we used displacement control and a data acquisition frequency of 20 Hz. Table S1 (Supporting Information) contains material properties of the base materials summarizing mean values and standard deviations.

5.3. Fracture Testing

To characterize the fracture behavior of the base materials and that of the composite materials, we performed fracture toughness tests on

single-edge-notched specimens under a mainly tensile loading. All the specimens have the same geometry and size ($80 \times 80 \times 3$ mm). In the case of stiffer samples, we cut the notch by means of a diamond-coated slitting saw. In the case of more compliant samples, we adopted a band saw. In all the cases, the notch length is 20% of the specimens' width. At the specimens' ends we glued aluminum tabs, to avoid stress concentration at the grips.

We tested the stiff material using an MTS RF-810 hydraulic machine, endowed with hydraulic grips and a 100 kN load cell. For the soft materials and the composite ones, we used an MTS Synergie 200 universal tensile testing machine, endowed with mechanical grips and a 1 kN load cell. We carried out the at least three fracture toughness tests for each material topology, under displacement control, using a $3\,\mathrm{mm\,min^{-1}}$ crosshead speed and a 20 Hz data acquisition frequency. Table S2 (Supporting Information) contains the mechanical properties resulted from the fracture tests performed on the base materials and on the composites, summarizing mean values and standard deviations.

For these tests, we did not follow reference standards. However, we paid attention to use the same geometry and loading conditions, to allow a final comparison on the fracture response and on the failure modes of the composites and the base materials. Although we applied tensile loading to all the fracture samples, we noticed that in some cases (i.e., compliant materials and composites), the samples underwent high deformation, leading to a more complex stress state, including a bending moment, due to the eccentricity of the load. The effect could be of reducing the final mechanical property of the materials (toughness and strength) as a more critical stress state arose, due to the combination of tensile and bending loading. However, being the tests setup and the sample geometry the same for all the samples, this effect was present in all the tests, likewise allowing a comparison of the results.

Article first published online: May 23, 2016
Manuscript Revised: April 7, 2016
Manuscript Received: March 16, 2016

[1] M. Milwich, T. Speck, O. Speck, T. Stegmaier, H. Planck, *Am. J. Bot*. **2006**, *93*, 1455.
[2] B. Bhushan, *Philos. Trans. R. Soc. A: Math. Phys. Eng. Sci*. **2009**, *367*, 1445.
[3] Z. Y. Tang, N. A. Kotov, S. Magonov, B. Ozturk, *Nat. Mater.* **2003**, *2*, 413.
[4] U. G. K. Wegst, H. Bai, E. Saiz, A. P. Tomsia, R. O. Ritchie, *Nat. Mater.* **2015**, *14*, 23.
[5] H. Bai, F. Walsh, B. Gludovatz, B. Delattre, C. Huang, Y. Chen, A. P. Tomsia, R. O. Ritchie, *Adv. Mater.* **2016**, *28*, 50.
[6] K. Chen, B. Shi, Y. Yue, J. Qi, L. Guo, *ACS Nano* **2015**, *9*, 8165.
[7] B. G. Compton, J. A. Lewis, *Adv. Mater.* **2014**, *26*, 5930.
[8] G. M. Luz, J. F. Mano, *Compos. Sci. Technol*. **2010**, *70*, 1777.
[9] L. J. Bonderer, A. R. Studart, L. J. Gauckler, *Science* **2008**, *319*, 1069.
[10] A. R. Studart, *Adv. Mater.* **2012**, *24*, 5024.
[11] C. Ortiz, M. C. Boyce, *Science* **2008**, *319*, 1053.
[12] X. Gu G, I. Su, S. Sharma, J. L. Voros, Z. Qin, M. J. Buehler, *ASME. J. Biomech. Eng*. **2016**, *138*, 021006-021006-16. DOI: 10.1115/1.4032423.
[13] M. D. Bartlett, A. B. Croll, D. R. King, B. M. Paret, D. J. Irschick, A. J. Crosby, *Adv. Mater.* **2012**, *24*, 1078.
[14] K. Autumn, Y. A. Liang, S. T. Hsieh, W. Zesch, W. P. Chan, T. W. Kenny, R. Fearing, R. J. Full, *Nature* **2000**, *405*, 681.
[15] N. A. Patankar, *Langmuir* **2004**, *20*, 8209.
[16] B. Bhushan, *Beilstein J. Nanotechnol*. **2011**, *2*, 66.
[17] F. Barthelat, R. Rabiei, *J. Mech. Phys. Solids* **2011**, *59*, 829.
[18] P. Fratzl, R. Weinkamer, *Prog. Mater. Sci*. **2007**, *52*, 1263.
[19] D. Sen, M. J. Buehler, *Sci. Rep*. **2011**, *1*, 35.
[20] P. Fratzl, *J. R. Soc. Interface* **2007**, *4*, 637.
[21] M. A. Meyers, J. McKittrick, P.-Y. Chen, *Science* **2013**, *339*, 773.
[22] M. J. Buehler, H. M. Yao, B. H. Ji, H. J. Gao, *Mech. Prop. Bioinspired Biol. Mater.* **2005**, *844*, 207.
[23] H. Gao, B. Ji, I. L. Jager, E. Arzt, P. Fratzl, *Proc. Natl. Acad. Sci*. **2003**, *100*, 5597.
[24] P. Fratzl, H. S. Gupta, *Nanoscale Mechanisms of Bone Deformation and Fracture*, Handbook of Biomineralization, ed. Bäuerlein. Vol. 1, Wiley VCH, Weinheim, Germany **2007**.
[25] E. Hamed, Y. Lee, I. Jasiuk, *Acta Mech*. **2010**, *213*, 131.
[26] S. Deville, E. Saiz, R. K. Nalla, A. P. Tomsia, *Science* **2006**, *311*, 515.
[27] S. Deville, E. Saiz, A. P. Tomsia, *Acta Mater.* **2007**, *55*, 1965.
[28] V. Naglieri, B. Gludovatz, A. P. Tomsia, R. O. Ritchie, *Acta Mater.* **2015**, *98*, 141.
[29] F. Libonati, C. Colombo, L. Vergani, *Fatigue Fract. Eng. Mater. Struct*. **2014**, *37*, 772.
[30] L. S. Dimas, G. H. Bratzel, I. Eylon, M. J. Buehler, *Adv. Funct. Mater.* **2013**, *23*, 4629.
[31] E. Lin, Y. Li, C. Ortiz, M. C. Boyce, *J. Mech. Phys. Solids* **2014**, *73*, 166.
[32] P. Zhang, M. A. Heyne, A. C. To, *J. Mech. Phys. Solids* **2015**, *83*, 285.
[33] Z. Qin, B. G. Compton, J. A. Lewis, M. J. Buehler, *Nat. Commun*. **2015**, *6*, 7038.
[34] S. V. Murphy, A. Atala, *Nat. Biotech*. **2014**, *32*, 773.
[35] M. Nakamura, S. Iwanaga, C. Henmi, K. Arai, Y. Nishiyama, *Biofabrication* **2010**, *2*, 014110.
[36] P. Fratzl, *Nat. Mater.* **2008**, *7*, 610.
[37] R. O. Ritchie, M. J. Buehler, P. Hansma, *Phys. Today* **2009**, *62*, 41.
[38] A. A. Abdel-Wahab, A. R. Maligno, V. V. Silberschmidt, *Comput. Mater. Sci.* **2012**, *52*, 128.
[39] K. J. Koester, J. W. Ager, R. O. Ritchie, *Nat. Mater.* **2008**, *7*, 672.
[40] F. Libonati, L. Vergani, *Composite Structures*, **2016**, *139*, 188. http://dx.doi.org/10.1016/j.compstruct.2015.12.003.
[41] R. Shahar, M. N. Dean, *BoneKEy Rep*. **2013**, *2*, 343.

[42] K. Tai, M. Dao, S. Suresh, A. Palazoglu, C. Ortiz, *Nat. Mater.* **2007**, *6*, 454.
[43] S. Yamada, S. Tadano, K. Fujisaki, Y. Kodaki, *J. Biomech.* **2013**, *46*, 31.
[44] L. S. Dimas, M. J. Buehler, *Bioinspiration Biomimetics* **2012**, *7*, 036024.
[45] C. Hennig, C. D. L. Thomas, J. G. Clement, D. M. L. Cooper, *J. Anat.* **2015**, *227*, 497.
[46] Stratasys. *Digital Materials*. Available from: http://www.stratasys.com/materials/polyjet/digital-materials
[47] ASTM, D638 − *Standard Test Method for Tensile Properties of Plastics*, ASTM International, West Conshohocken, PA **2010**.
[48] ASTM, D412 − *Standard Test Methods for Vulcanized Rubber and Thermoplastic Elastomers—Tension*, ASTM International, West Conshohocken, PA **2013**.